

Thermal plant based on parabolic trough collectors for industrial process heat generation in Morocco



Badreddine El Ghazzani ^{a,*}, Diego Martinez Plaza ^b, Radia Ait El Cadi ^a, Ahmed Ihlal ^a, Brahim Abnay ^c, Khalid Bouabid ^a

^a Materials and Renewable Energies Laboratory, Faculty of Science, IbnZohr University, BP8106, 80006, Agadir, Morocco

^b Plataforma Solar de Almeria (PSA-CIEMAT), P.O. Box 22, 04200, Tabernas, Almeria, Spain

^c Ciment du Maroc, Usine d'Ait-Baha, Route Principale 1007 km 10, Commune ImiMqorn, Morocco

ARTICLE INFO

Article history:

Received 31 January 2017

Received in revised form

24 May 2017

Accepted 18 June 2017

Available online 20 June 2017

Keywords:

Dynamic simulation

Parabolic trough

Industrial process heat

Exergy

TRNSYS

ABSTRACT

In the last decades, solar thermal power plants based on parabolic trough concentrators have been widely deployed in the industry sectors. Indeed, there are various applications for thermal plants in industry, such as desalination, refrigeration and air heating. In this work, a dynamic simulation of a small sized parabolic trough collector plant is conducted, using TRNSYS software, for the purpose of generating heated air for an industrial factory. In order to analyze the configuration proposed for this plant, the selected case study is a food industry which requires heated air at 150 °C (medium range temperature) during a daily operation time 8:30 to 00:00 h, throughout the year. The simulation is conducted under Moroccan meteorological conditions in order to encourage the use of this technology in this country. The design and control of the plant are presented and the simulation results are analyzed on different time bases illustrating energetic and exergetic performance data. The environmental impact has been analyzed by focusing on the amount of CO₂ emissions resulting of the natural gas combustion at the auxiliary heater subsystem. Calculations determine that up of 57% of CO₂ emissions can be avoided annually by the implementation of the solar plant.

© 2017 Elsevier Ltd. All rights reserved.

1. Introduction

The continuous evolution of the global industry is accompanied by a sharp increase in energy demand. Heat, for industrial purposes, constitutes a large part of this energy. Thus, in order to cover this need, renewable energies can be a reliable solution, instead of the classic energy sources [1]. About half of the energy consumption can be provided by solar thermal in developed economies by supplying hot water and steam in a temperature range of up to 400 °C. In developing countries, especially for agriculture, textile, food and other industries, solar thermal energy can provide hot air and hot water needed for curing, drying, washing, boiling, sterilization and pasteurization [2]. Most industrial process heat demand requires heat in temperature ranges that can be provided by a solar thermal system. Industrial solar process heat installations require thermal energy in the 'low' ($T < 150$ °C) or 'medium' temperature ranges (150 °C $< T < 400$ °C) [3].

The percentage of thermal energy demand in the low temperature range is extremely higher in food, beverages, paper and textile industries, while plastics and chemical industries need it in medium temperature range mostly. These industries require more than 50% of their total process heat in the temperature range up to 250 °C for such diverse applications as drying, cleaning, extraction and many others. Broadly speaking, paper and food industries are the most energy intensive ones, while textile and chemical industries have also a considerable heat demand [4].

Concentrated solar power (CSP) systems convert the energy from the sun into consumable power such as electricity [5], it is considered as the main technology used for medium temperature [6]. For industrial process heat and power generation, solar parabolic trough collectors (PTC) [7] constitute a proven CSP device for thermal energy supply. Generally, the PTC is composed of an absorber which is fixed at the focus of a parabolic concentrator; the absorber is covered by a concentric transparent cover in the purpose of decreasing the heat losses.

All over the world around 140 solar thermal plants for industrial applications were reported in 2014 with a total capacity of over

* Corresponding author.

E-mail addresses: b.elghazzani@yahoo.com, badreddine.elghazzani@edu.uiz.ac.ma (B. El Ghazzani).

Nomenclature

A	collector's aperture area
$C_{fl,cold}$	capacity rate of HTF on cold side
$C_{fl,hot}$	capacity rate of HTF on hot side
C_{max}	maximum capacity rate
C_{min}	minimum capacity rate
C_r	ratio between the lower and higher capacity
C_p	thermal capacity
Ex	exergy
$F_R(\tau\alpha)_n$	absorption efficiency of solar radiation by the plate
$F_R U_L$	collector loss rate
f_{solar}	solar fraction
I_b	Direct incident radiation (beam)
IR_{sf}	irreversibility of the solar collector field
m	mass
\dot{m}	mass flow rate
Q	energy
\dot{Q}	energy by unit of time
\dot{Q}_i	total incident solar energy received by the collector's aperture area
\dot{Q}_u	total useful energy delivered by the solar field
S	entropy
T	temperature
t	time
UA	overall heat transfer coefficient
V	Volume

Greek symbols

ρ	density
θ	angle of incidence
η	efficiency
$\eta_{I,sf}$	efficiency of the collector field
$\eta_{II,sf}$	exergy efficiency of the solar collectors field
ΔT	temperature difference
Δ	change

Subscript

air	air
am	ambient
aux	auxiliary heater system

avr	average
$coll$	collector field
$cold$	cold
ch	charging
$dest$	destruction
dis	discharging
$exch$	exchanger
fl	heat transfer fluid (HTF)
h	high temperature
hot	hot
i, j	serial numbers
in	inlet
l	low temperature
$load$	load
$loss$	heat loss
min	minimum
max	maximum
out	outlet
rec	recovering
set	set point
sf	solar collector field
str	storage
sun	the sun
$tank$	storage tank
t	thermal
u	useful from parabolic field

Abbreviation

CSP	concentrating solar power
DNI	direct normal irradiance
EIA	energy information administration
IEA	international energy agency
$NREL$	national renewable energy laboratory
HTF	heat transfer fluid
IAM	incidence angle modifier
NUT	number of transfer unit
$ONHYM$	national office of hydrocarbons and mines (Morocco)
PTC	parabolic trough collector
TES	thermal energy storage
$TESS$	thermal energy systems specialists
TMY	typical meteorological year

93 MWth (>136 000 m²). The most of these plants are small-scale pilot projects. Only 18 plants have collector areas larger than 1000 m² [8]. In Morocco, the solar thermal is a growing sector. The meteorological conditions are actually favorable with a direct normal irradiance (DNI) exceeding 2500 kWh/m² in large areas of the country. CSP has become an emergent technology, in Morocco, with several plants already operational while others are under construction, as it is mentioned on the NREL [9] website and presented in Fig. 1. PTC is the most used technology in this country, which hosts the world biggest CSP plant since 2015, NOOR-I. All the existing or planned plants are for the electricity generation. We aim to take full advantage of the country's climate conditions and encourage industries to incorporate CSP technology in their processes in order to phase-out fossil fuels as much as possible.

Numerous studies have treated the design performance issues of solar PTC structures and parabolic concentrators. Edenburn [10] have conducted a performance study on a parabolic trough collector comparing a theoretical evaluation and the experimental results. Rojas et al. [11] have presented a description of a capillary

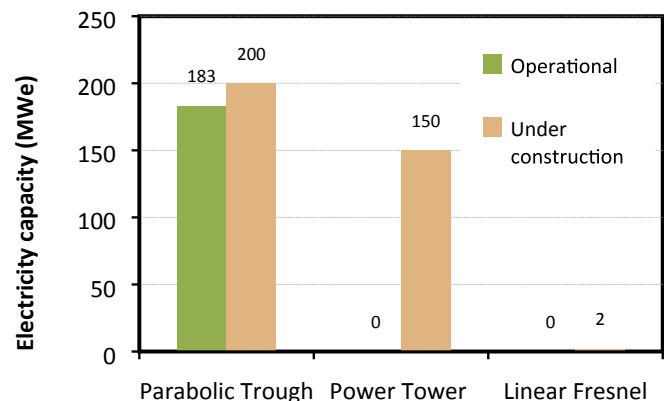


Fig. 1. Moroccan CSP capacity by December 2015 as in NREL <http://www.nrel.gov/csp/solarpaces/> [9].

system (etched micro-channels or a porous coating) to be integrated into LS3 receivers. Naeni and Yaghoubi [12] have focused on wind flow analysis on PTC by varying the orientation of the collector with different wind velocities. Also, several researchers have studied how to improve the thermal efficiency of the PTCs. Bakos [13] has conducted an experimental study on a two axis sun tracking system for PTC, and he has compared the thermal efficiency of the classic collector with the moving surface. Jeter [14] focused his investigations on the optical behavior of the PTC. He conducted an analysis by considering parameters such as concentration ratio for absorber and concentrated flow density. You et al. [15] have conducted a heat transfer and flow analysis in PTCs used at a direct steam generation (DSG) system using the finite difference method.

Several works studied the use of thermal systems based on solar PTCs coupled with organic Rankine cycle (ORC) for electrical power production. Quoilin et al. [16] have designed a solar ORC for rural electrification purposes. The system consists of parabolic trough collectors, a storage tank and a small-scale ORC engine using scroll expanders. They developed a model of each component based on experimental data for the main key components in order to evaluate the performance of the system. Al-Sulaiman et al. [17] have presented the performance assessment of a novel system based on parabolic trough solar collectors plus ORC for combined cooling, heating and power (CCHP). In their system they considered that a portion of waste heat is used for heating through a heat exchanger and the other portion is used for cooling through a single-effect absorption chiller. He et al. [18] conducted a simulation with the transient energy simulation package TRNSYS [19]. They established a model for a typical parabolic trough solar thermal power generation system with ORC. In their modeling they considered several sub-models for the trough collector system and they examined the effect of several parameters on the performance of the solar field. Borunda et al. [20] have presented a study of a small CSP plant coupled to an ORC with a configuration where energy is directly used to feed the power block and to charge the thermal storage, the performance of the solar power plant was simulated with TRNSYS software.

On the other hand, a few studies have assessed the feasibility of incorporating a solar thermal plant into industrial processes as a source of thermal energy, mainly as hot air, water or steam. In this context, Kalogirou [21] had investigated in 2001 the viability of using parabolic trough collectors for industrial process heat generation in Cyprus. The system investigated consisting of an array of parabolic trough collectors, hot water storage tank, piping, and controls was modeled with TRNSYS. Kalogirou [4] in 2002 had analyzed industrial process heat systems concerning the life-cycle savings, energy yield and the resulting thermal energy price for a number of collector technologies and demand temperatures. The obtained results for this study are applicable to any country with similar weather and economic conditions as Cyprus where the study was conducted. Recently in 2013 Silva et al. [22] have developed a tri-dimensional non-linear dynamic thermo-hydraulic model of a PTC in object-oriented language *Modelica* and they have coupled it to a solar industrial process heat plant modeled in TRNSYS. In 2014 Silva et al. [2] have studied the use of a PTC plant to generate saturated steam for a canned vegetables industry located in Southern Spain.

In this work, we have used the transient energy simulation package TRNSYS [19] to simulate the performance of a PTC station to supply hot air to an existing industrial process. The station contains also a storage system and an auxiliary heating system; both of them are connected to the solar field. The required air temperature at the output of the heat exchanger is assumed to be 150 °C, during the daily operating time of the factory, from 8:30 h to

midnight, throughout the year.

2. System description

The aim of this work is to assess the operation of a solar plant based on small-sized parabolic trough collectors for industrial heat processes under the Moroccan meteorological conditions. A schematic diagram of the plant is shown in Fig. 2. It consists essentially of the solar collector field, the thermal storage single-tank, the regulation tank which is a smaller secondary tank and the auxiliary heater subsystem, all these components are coupled to a heat exchanger subsystem.

When the insolation is enough to drive the process, the solar field heats up the oil that flows through the receivers of the collectors so it feeds constantly the storage tank. By night or when the sky is non-clear and DNI is low, the flow of heat transfer fluid (HTF) is stopped by the temperature controller C1. This controller receives temperature signals from thermal sensors, TS1 that is implemented at the solar field outlet, and TS2 at the storage tank bottom. When the temperature difference between the tank top inlet and bottom outlet is lower than 10 °C the pump P1 is set off and the flow stops in this loop. The thermal sensor TS3 watches HTF temperature at tank outlet feeding the load via the valve V1 and send signals to the controller C3 that commands Pump P3, making a fraction of HTF goes through the regulation tank with the purpose to store heat into it when the temperature of the oil at the valve V1 inlet is higher than the set point in the load. Pump P2 is controlled so that the station operates according to the desired time. Fig. 3 shows the flowchart for the operation of the plant.

3. Thermodynamic analysis and models formulations

Formulations for mathematical models of each plant component are expressed in this section. Steady-state operation of all subsystems and negligible kinetic and potential energy changes are assumptions to carry out the thermodynamic analysis.

3.1. Parabolic trough collector field

3.1.1. Energy analysis

The total solar energy received by solar field aperture area is given by the equation,

$$\dot{Q}_i = I_b \cdot A \cdot \cos \theta \quad (1)$$

The collector performance is given by the following equation [23],

$$\dot{Q}_u = A [F_R(\tau\alpha)_n I_b - F_R U_L (T_{in} - T_{am})] \quad (2)$$

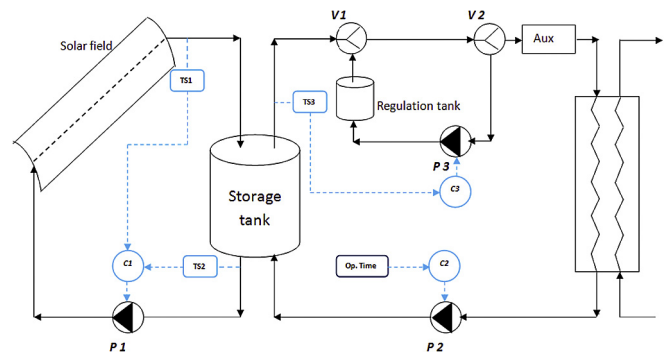


Fig. 2. The scheme of the solar plant.

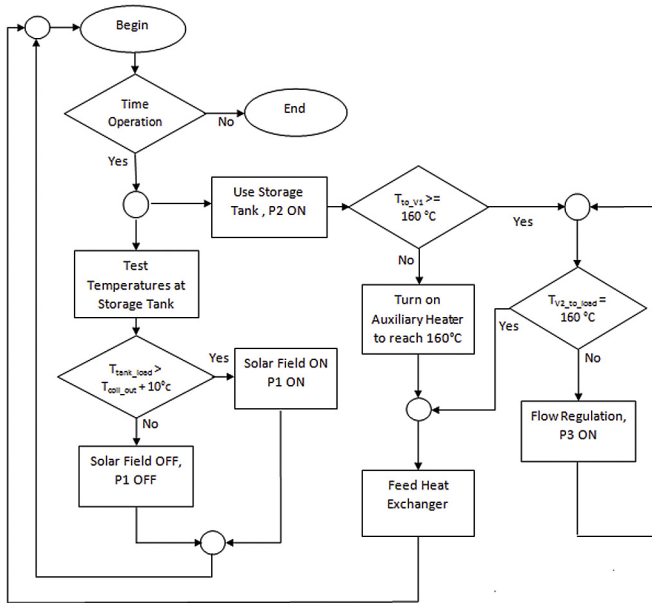


Fig. 3. Flowchart of the solar thermal plant operation.

where \dot{Q}_i is the energy received by the solar field, \dot{Q}_u is the useful gain of the collector, A is the aperture area of the solar field, it is represented by the addition of areas formed by the mouth of the parabolic reflector and the length of each single collector tube, $F_R(\tau\alpha)_n$ is the efficiency with which solar radiation is absorbed by the plate and removed by fluid flowing through the collector, I_b is the amount of beam solar radiation incident on the plane of the collector surface, $F_R U_L$ is the collector loss rate, T_{in} is the temperature of the fluid entering the collector array and T_{am} is the ambient temperature of the collector's surroundings.

While the temperature of the fluid at the collector outlet is given by the equation,

$$T_{out} = T_{in} + \frac{\dot{Q}_u}{\dot{m}_f C_{p_f}} \quad (3)$$

Thus the energy efficiency of the solar field is presented as,

$$\eta_{l, sf} = \frac{\dot{Q}_u}{\dot{Q}_i} \quad (4)$$

3.1.2. Exergy analysis

The quantitative energy losses involved in various components of the system can be given by the energy analysis, whereas to describe qualitatively the system the second law of thermodynamic is necessary. Exergy analysis gives the qualitative energy losses by using the conservation of mass and conservation of energy principles together with the second law of thermodynamics. In this subsection, the performance of solar thermal field is analyzed in terms of exergy efficiencies, the analysis is based on the following references [20,24–28].

The exergy received by the collector, consist of the exergy delivered from the solar radiation, it is given by Petela theorem that is expressed by:

$$Ex_{sun} = \dot{Q}_i \left(1 - \frac{T_{am}}{T_{sun}} \right) \quad (5)$$

where T_{sun} is the apparent temperature of the sun estimated by 3/4 of the black body temperature, it is about 4077 °C [29], and T_{am} is

the ambient temperature. The available exergy of the solar field involves the exergy supplied from the solar radiation added to the auxiliary heater exergy and is given by:

$$Ex_{sf} = \dot{Q}_i \left(1 - \frac{T_{am}}{T_s} \right) + \dot{Q}_{aux} \left(1 - \frac{T_{am}}{T_{fl}} \right) \quad (6)$$

The exergy received by the heat transfer fluid in the parabolic trough collectors can be written as:

$$Ex_U = N \dot{m}_f [(h_{out} - h_{in}) - T_{am}(S_{out} - S_{in})]_{coll} = \dot{Q}_U \left(1 - \frac{T_{am}}{T_{out}} \right) \quad (7)$$

where (\dot{Q}_U) is the heat gain of the collector is described by equation (2), N is the number of collectors in the field, and \dot{m}_f is the mass flow rate of the HTF in the solar field, h_{in} and h_{out} are enthalpies at the inlet and outlet and S_{in} , S_{out} are entropies.

The exergy efficiency of the solar collector field can be described by:

$$\eta_{II, sf_0} = \frac{\dot{Q}_U \left(1 - \frac{T_{am}}{T_{out}} \right)}{\dot{Q}_i \left(1 - \frac{T_{am}}{T_s} \right)} \quad (8)$$

In the presence of one auxiliary heater, the efficiency of the solar field can be written as:

$$\eta_{II, sf1} = \frac{\dot{Q}_U \left(1 - \frac{T_{am}}{T_{out}} \right)}{\dot{Q}_i \left(1 - \frac{T_{am}}{T_s} \right) + \dot{Q}_{aux} \left(1 - \frac{T_{am}}{T_{fl}} \right)} \quad (9)$$

The irreversibility of the solar collector field is calculated by:

$$IR_{sf} = Ex_{sf} - Ex_U = \dot{Q}_i \left(1 - \frac{T_{am}}{T_{sun}} \right) - \dot{Q}_U \left(1 - \frac{T_{am}}{T_{out}} \right) \quad (10)$$

And the entropy rate in the collectors system is described by:

$$S_{sf} = \frac{\dot{Q}_{loss}}{T_{am}} + \frac{\dot{Q}_U}{T_{fl}} - \frac{\dot{Q}_i}{T_{sun}} \text{ with } \dot{Q}_U = \dot{m}(h_{out} - h_{in})_{coll} \quad (11)$$

3.2. Thermal storage tank

The thermal energy storage (TES) can solve the mismatch between the solar energy supply and load demand. It can be used to extend the plant's operating time in low radiation or night time. There are different ways to store thermal energy for CSP systems, it can be stored in sensible heat storage by using either solid or liquid media, thermochemical storage through chemical reactions and latent heat storage by using phase change materials [30]. Instead of the two-tank molten salt sensible storage which is the most commonly used storage technique in CSP plants [31], a single tank thermocline system can be used, therefore the hot and cold fluids are stored in the same tank and separated due to the thermal stratification [32].

A single tank thermocline scheme is adopted for this study and Thermintol 62, the heat transfer fluid is used also as the heat storage medium. The heat transfer process inside the single tank is simulated by the thermocline model, a model where the tank is divided into 'n' units with equal volume from the top to the bottom Fig. 4. The degree of stratification of the tank is determined by the value of 'n'. In order to simplify the model we assume that the distribution of temperature is uniform in each unit, the heat conduction is

ignored between adjacent units and the flow rate of the HTF is neglected because of the large volume of the tank. It is an existing model in TRNSYS [19].

3.2.1. Storage tank mathematical model

The energy balance in the *i*th unit can be generally expressed as:

$$\begin{aligned} \dot{m}_{fl,i} C_{pfl,i} \frac{dT_{fl,i}}{dt} = & a_i \dot{m}_{fl,i} C_{pfl,i} (T_{fl,h} - T_{fl,i}) + b_i \dot{m}_{fl,i} C_{pfl,i} (T_{fl,L} \\ & - T_{fl,i}) + U_{str-am} A_{str,i} (T_{fl,i} - T_{am}) \\ & + \begin{cases} C_i (T_{i-1} - T_i) C_{pfl,i} & C_i > 0 \\ C_i (T_i - T_{i+1}) C_{pfl,i} & C_i < 0 \end{cases} \end{aligned} \quad (12)$$

where $\dot{m}_{fl,i}$, $C_{pfl,i}$, are respectively the mass flow and constant specific pressure heat of the HTF in the *i*th unit and $T_{fl,i}$ is the *i*th temperature. T_{am} is the environment temperature, $A_{str,i}$ is the surface area of the *i*th element and U_{str-am} is the overall heat transfer coefficient between the tank and the environment. The constants a_i , b_i , C_i are control functions and are given by:

$$a_i = \begin{cases} 1, & i = S_h \\ 0, & i \neq S_h \end{cases} \quad (13)$$

$$b_i = \begin{cases} 1, & i = S_l \\ 0, & i \neq S_l \end{cases} \quad (14)$$

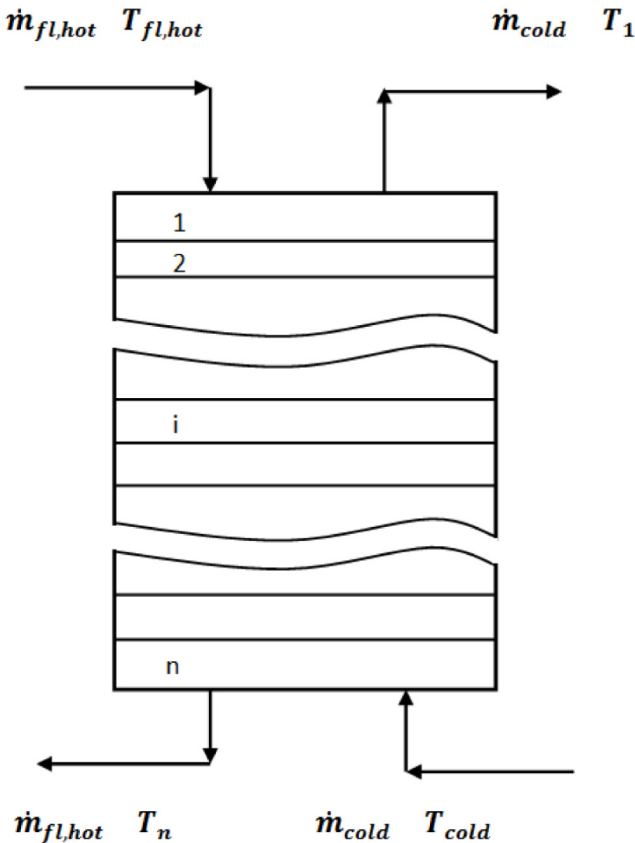


Fig. 4. Scheme of the storage single-tank.

$$C_i = \dot{m}_{fl,h} \sum_{j=1}^{i-1} a_j - \dot{m}_{fl,h} \sum_{j=i+1}^n b_j \quad (15)$$

The HTF flows from collectors field and the heat exchanger into a number of control volume denoted respectively by S_h and S_l .

Energy flows and change in internal energy are calculated as follows:

$$Q_{loss,str} = \sum_{i=1}^n U_{str-am} A_{str,i} (T_{fl,i} - T_{am}) \quad (16)$$

$$Q_{coll-str} = \dot{m}_{fl,h} \frac{\sum_{i=1}^n C_{pfl,i}}{n} (T_{fl,h} - T_{fl,n}) \quad (17)$$

$$\Delta E = \sum_{i=1}^n \dot{m}_{fl,i} \cdot \frac{\sum_{i=1}^n C_{pfl,i}}{n} \cdot \frac{(\sum_{i=1}^n T_i - \sum_{i=1}^n T_i|_{t=0})}{n} \quad (18)$$

where $Q_{loss,str}$ is the heat loss in the storage tank, $Q_{col-str}$ the heat transferred by the HTF from the collector field to the storage tank, and ΔE the thermodynamic energy change in the storage tank.

3.2.2. Storage tank exergy analysis

The thermal storage tank is analyzed in terms of exergy efficiencies, the analysis is based on the following references [20,24–28].

The storage tank exergy does not contribute to the solar field exergy, however, the solar field exergy is considered to establish the exergy of the TES.

The overall exergy balance for the storage tank during an overall cycle is written as:

$$Ex_U - (Ex_{rec} + Ex_{loss}) - Ex_{dest} = Ex_{\Delta} \quad (19)$$

where Δ is the change in the exergy accumulation.

The operating mode of the TES can be described following the three operating stages; charging, storing and discharging.

During the charging stage, the energy collected by the solar field is transferred to the TES via the HTF, hence an exergy balance for the TES subsystem can be expressed as:

$$Ex_U - Ex_{dest} - Ex_{loss} = Ex_{\Delta,Ch} \quad (20)$$

where Ex_U is the exergy delivered by the PTC field (equation (7)), Ex_{dest} is the exergy destruction, Ex_{loss} is the exergy loss, and $Ex_{\Delta,Ch}$ is the exergy accumulation during the charging time.

The exergy efficiency of the TES during the charging stage is described by:

$$\eta_{II,Ch} = \frac{Ex_{\Delta,Ch}}{Ex_U} \quad (21)$$

The storing stage is an intermediate period where the TES store energy without charging or discharging. The exergy balance for the storing stage is expressed as:

$$-Ex_{loss} - Ex_{dest} = Ex_{\Delta,Str} \quad (22)$$

where $Ex_{\Delta,Str}$ is the storage exergy.

The efficiency of the storing stage is written as:

$$\eta_{II,Str} = \frac{Ex_{\Delta,Str}}{Ex_{\Delta,Ch}} \quad (23)$$

The discharging stage is the period where the stored energy in

the TES is recovered to be used. The exergy balance at this stage is presented as:

$$-(Ex_{rec} + Ex_{loss}) - Ex_{dest} = Ex_{\Delta,dis} \quad (24)$$

where Ex_{rec} is the exergy recovered to use at the heat exchanger, $Ex_{\Delta,dis}$ is the exergy accumulation during the discharging stage period.

The exergy efficiency of the discharging stage period is described by:

$$\eta_{II,Dis} = \frac{Ex_{rec}}{Ex_{\Delta,Str}} \quad (25)$$

Therefore, Then the overall exergy efficiency at the thermal storage tank can be expressed by:

$$\eta_{II,tank} = (\eta_{II,Ch})(\eta_{II,Str})(\eta_{II,dis}) = \frac{Ex_{rec}}{Ex_U} \quad (26)$$

$$\eta_{II,tank} = \frac{Q_{rec} \left(1 - \frac{T_{am}}{T_{rec}}\right)}{Q_U \left(1 - \frac{T_{am}}{T_{out}}\right)} \quad (27)$$

where Q_{rec} is the recovered energy from the TES, Q_U is the energy delivered by the solar field, T_{am} is the ambient temperature, T_{rec} is the temperature of the HTF recovered to use and T_{out} is the temperature at the solar field outlet.

3.3. The auxiliary heater subsystem

3.3.1. The mathematical model of the auxiliary heater

The prolongation of the plant's operating time is often needed when the solar radiation is too low and the heat energy in the thermal storage system is exhausted, a continuous and stable operation can be reached just by the incorporation of an auxiliary heater system in the plant.

In the auxiliary heater system, T_{set} is the temperature at the outlet required by the load. The comparison between the temperature of HTF that flows into the auxiliary heater system and T_{set} , can decide the mode of operation of this auxiliary system. When $T_{avr,aux} > T_{set}$, the auxiliary heater system is off, therefore there is no energy delivered by the system either no heat loss, in the other case when $T_{avr,aux} < T_{set}$, the energy provided by the system (Q_{aux}) and the heat loss into it ($Q_{loss,aux}$) can be expressed, respectively as:

$$Q_{aux} = \frac{\dot{m}_{aux} Cp_{aux} (T_{set} - T_{aux}) + U_{aux-am} A_{aux} (T_{avr,aux} - T_{am})}{\eta_{aux}} \quad (28)$$

$$Q_{loss,aux} = U_{aux-am} A_{aux} (T_{aux} - T_{am}) + (1 - \eta_{aux}) \quad (29)$$

where \dot{m}_{aux} , Cp_{aux} , and $T_{avr,aux}$, are respectively the mass flow rate, the specific heat of the HTF in the auxiliary energy system and the average temperature. U_{aux-am} is the overall heat transfer coefficient between the auxiliary heater system and the environment. η_{aux} and A_{aux} are the efficiency of the auxiliary heater subsystem and its surface area, respectively.

3.3.2. Auxiliary heater exergy analysis

The auxiliary heater subsystem is analyzed in terms of exergy, the analysis is based on the following references [20,25,26,28].

The auxiliary heater is a contributor in the available exergy for the system. Its exergy is expressed by:

$$Ex_{aux} = Q_{aux} \left(1 - \frac{T_{am}}{T_{fl}}\right) \quad (30)$$

where Q_{aux} is the energy at the auxiliary heater, T_{am} is the ambient temperature and T_{fl} is the HTF temperature at the outlet of the auxiliary heater.

3.4. The heat exchanger subsystem

A counter current heat exchanger subsystem is used. The Number of Transfer Unit (NUT) efficiency model which is an existing model in TRNSYS is employed to simulate the heat exchanger subsystem.

3.4.1. The heat exchanger mathematical model

Equations demonstrating the heat transfer in a counter-flow configuration are shown below.

$$Q_{exch} = U_{exch} A_{exch} \Delta T_{exch,ml} \quad (31)$$

where,

$$\Delta T_{exch,ml} = \frac{\Delta T_{exch,max} - \Delta T_{exch,min}}{\ln\left(\frac{\Delta T_{exch,max}}{\Delta T_{exch,min}}\right)} \quad (32)$$

The heat rate into the heat exchanger can be also expressed by:

$$\dot{Q}_{exch} = \dot{m}_{air} \Delta h_{exch,air} = \dot{m}_{fl,exch} \Delta h_{fl,exch} \quad (33)$$

In each side of the heat exchanger, the capacitance can be calculated according to the following four equations.

$$C_{hot} = \dot{m}_{fl,hot} Cp_{fl,hot} \quad (34)$$

$$C_{cold} = \dot{m}_{fl,cold} Cp_{fl,cold} \quad (35)$$

$$C_r = \frac{C_{min}}{C_{max}} \quad (36)$$

where C_r is the ratio between the lower and higher capacity, NUT is the Number of Transfer Unit of the two fluids participating in the heat transfer.

$$NUT = \frac{U_{exch} A_{exch}}{C_{min}} \quad (37)$$

And finally the NUT efficiency is given as:

$$E_{exch} = \frac{1 - e^{-NUT(1-C_r)}}{1 - C_r e^{-NUT(1-C_r)}} \quad (38)$$

3.4.2. The exergy analysis of the heat exchanger

The analysis in terms of exergy of the heat exchanger subsystem is based on the following references [20,24,25,27,28].

The exergy of the heat exchanger subsystem is written as:

$$Ex_{exch} = \dot{Q}_{exch} \left(1 - \frac{T_{am}}{T_{fl}}\right) \quad (39)$$

where is T_{am} is the ambient temperature, T_{fl} is the HTF temperature at the inlet of the heat exchanger and \dot{Q}_{exch} is estimated heat considering the enthalpy difference between the inlet and the

outlet of the heat exchanger.

The second low efficiency of the heat exchanger is given by:

$$\eta_{II, TES} = \frac{\dot{Q}_{exch} \left(1 - \frac{T_{out}}{T_{in}}\right)}{\dot{Q}_U \left(1 - \frac{T_{out}}{T_{in}}\right)} \quad (40)$$

3.5. The plant efficiencies and solar fraction

Basing on references [20,24–28], the plant efficiencies and the solar fraction are carried out.

The plant thermal efficiency is described by:

$$\eta_{I,t} = \frac{\dot{Q}_{exch}}{(I_b * A) + \dot{Q}_{aux}} \quad (41)$$

The thermal second low efficiency of the plant is defined as:

$$\eta_{II,t} = \frac{\dot{Q}_{exch} \left(1 - \frac{T_a}{T_{in}}\right)}{(I_b * A) \left(1 - \frac{T_a}{T_{sun}}\right) + \dot{Q}_{aux} \left(1 - \frac{T_a}{T_{in}}\right)} \quad (42)$$

While the solar fraction is calculated by:

$$f_{solar} = \frac{\text{Solar input}}{\text{Solar input} + \text{Auxiliary input}} = \frac{\dot{Q}_{exch} - \dot{Q}_{aux}}{\dot{Q}_{exch}} \quad (43)$$

4. Environmental impacts and economic analysis

The importance of this kind of energy systems comes from their nature to be ecological; hence it is necessary to study the environmental impact of these systems, so we can talk about the land use, the water consumption and the life cycle gas emissions. The focus of our study is on the greenhouse emissions resulting from fuel combustion at the auxiliary heater subsystem.

Some earlier published works on the emissions generated during the life cycle of the solar plants based on the parabolic trough collectors have been reviewed [33–35], a large part of these emissions comes from the operation and maintenance of the plant which mainly consist of emissions that comes from electricity consumption from the grid with about 48,5 kg CO₂ eq/MWh. The auxiliary heater produces an important amount of CO₂ from natural gas combustion with about 95 kg/MWh as well as for its provision with 16,6 kg/MWh. (The functional unit here has been defined as the production of 1 MW h of electricity).

The organic combustion can release various pollutants like CO₂, SO_x, NO_x, and some trace elements into the atmosphere. Therefore the environmental impact of the auxiliary heater can be evaluated on the basis of thermal energy delivered to the HTF. Direct CO₂ emissions from fuels are directly related to the presence of carbon in their chemical formulations, thus it is possible to evaluate the ratio between CO₂ emissions and the energy emitted by combustion.

The industry sector is among the largest consumers of energy in Morocco with 26% of the total energy consumption. The fuels; oil, coal [36], and natural gas [37] which all represent 89.4% of the energy mix of Morocco, are used in this sector. Noting that Morocco is nearly 91% dependent on imported energy, this includes gas from Algeria, oil, oil products and coal from international markets, and electricity from Spain [38].

The quantity of CO₂ emissions that comes from the combustion of natural gas is estimated by 204 (kg CO₂ eq/MWh Lower heating

value (LHV)) while those coming from the combustion of coal are about 345 kg/MWh LHV furthermore, heating oil releases 272 kg/MWh LHV. Noting that LHV is the amount of heat released by the complete combustion of a fuel unit.

Considering that natural gas is a naturally occurring hydrocarbon gas mixture consisting primarily of methane, and coal is composed primarily of carbon, the amount of energy released by the combustion of the natural gas is about 13.9 kWh LHV per kilogram of fuel at 25 °C, whereas by the combustion of coal this amount is about 9.2 kWh LHV per kilogram of fuel at 25 °C.

Generally, the economical aspect is the most decisive part in the selection of the appropriate fuel for the auxiliary heater. A comparison between the costs of the natural gas and coal that might be consumed in the plant is conducted.

In Morocco, according to information published by the National Office of Hydrocarbons and Mines (ONHYM) [39], the average price of coal is 0.11 \$/kg and the average of natural gas price is about 0.278 \$/kg in 2012. Since there is no available newest fuels price information from an official organization in Morocco, U.S. fuel prices are used as inputs for this study and are available through the Energy Information Administration (EIA) [40] open data. The prices can be higher in Morocco, however, the difference between the two fuel prices could not be significant in the two countries.

According to EIA [40], in 2015, the average delivered price of coal to the industrial sector was \$65.44 per ton or \$0.06544 per kg. The average annual industrial price of the United States natural gas, in 2015, is (3.2 Dollars per Thousand Cubic Feet or \$0.113 per m³). Knowing that for natural gas, 1 kg (kg) = 1.15 cubic meters (m³) at 25 °C and atmospheric pressure, therefore the price is \$0.13 per kg.

5. Assumptions, boundary conditions and methodology

The simulation of the plant is realized by giving a complete technical description and detailed characteristics of each subsystem, selecting a suitable site and imposing boundary conditions and assumptions for the system.

5.1. Meteorological data

The typical meteorological year (TMY) represents selected meteorological data for a specific location. These data are specially selected in order to present the range of weather events in a specific area by giving the average annual data that are compatible with long-term averages for that location.

The prediction of the solar field thermal power during a typical year require hourly DNI data, while ambient temperature, wind speed, and relative humidity are used to simulate solar field thermal performances [41]. According to the objective of our study that lies in encouraging industries in Morocco to adopt the parabolic trough plant for industrial process heat, the selected location to assess annual performance of the plant is Agadir. Ait-Baha site is located southwest of Morocco (Latitude 30,223°N; Longitude -9157°E; Altitude 254 m) and is characterized by an adequate climate in terms of insolation for thermal power plants and it is considered as a second industrial zone of the Agadir region. In this location, the DNI is mostly greater than 2100 kJ/h. m², the mean ambient temperature is 23 °C and the mean value of wind speed is about 3.4 m/s, Fig. 5 shows the variation of global solar irradiation and DNI throughout the year (8760 h/31 536 000 s) for Agadir Ait-Baha site, the wind speed and humidity variation is represented in Fig. 6, whereas the hourly ambient temperature variation is shown in Fig. 7.

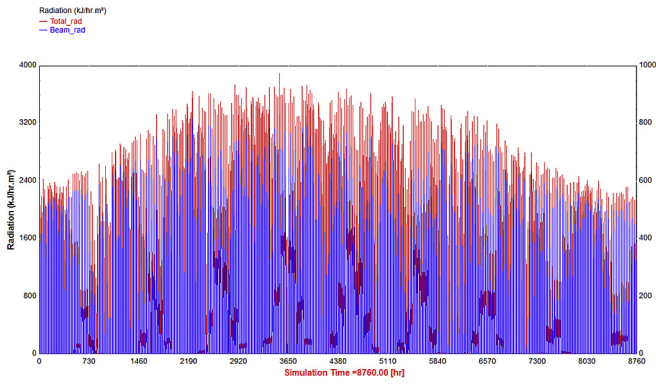


Fig. 5. Global solar irradiation and DNI throughout the year.

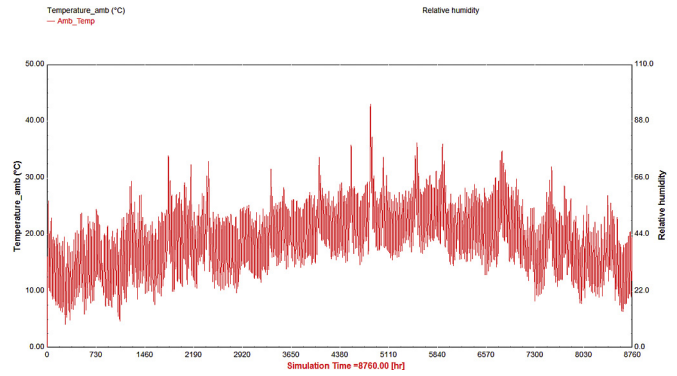


Fig. 7. Evolution of ambient temperature throughout the year.

5.2. Solar field

5.2.1. Features of the collectors used

Small-sized parabolic trough collectors are designed to be easily mounted on the ground as well as on roofs, which can be a good solution to save land surface, and developed for high performance for the medium temperature range. The solar parabolic trough “PolyTrough 1200” of the commercial brand NEPsolar [42] are employed for this study. Table 1 shows the main features of this device.

The evolution of the incidence angle modifier IAM of the collector as a function of the radiation incidence angle on its aperture, as given by the manufacturer is illustrated in Fig. 8:

5.2.2. Features of heat transfer fluid (HTF)

The heat transfer fluid (HTF) selected is Therminol 62 [43]. This synthetic oil flows through each collector and also used as the medium of the thermal storage energy in the storage tank. Therminol 62 is fouling resistant oil which can be used in a large interval of temperature (−25 to 325 °C), it is designed, according to the manufacturer, to provide reliable performances for many usage years when operating at the recommended range of temperature. The main properties of Therminol 62 are presented in Table 2.

5.3. Methodology and case study

As mentioned earlier, the aim of this study is to show the operation of parabolic trough plant which the schematic diagram is shown in Fig. 1. Since the heat demand is high in the medium temperature range for diverse applications in different fields of industry, we assume conducting a simulation in order to produce

heated air for industrial application at 150 °C, under the meteorological conditions of Agadir. Ait-Baha site in Morocco, this site that currently hosts some industrial factories and could host others in the future.

A case of a food industry is considered, this factory starts operation at 8.30 a.m., for 13 h and a half every day all over the year, with heated air temperature demand of 150 °C.

The choice of components is done taking into account the state of the market, the components should be commercially available and have a good quality/price ratio, therefore basing on technical specifications of these components and the selection of the HTF, the dimensioning of the plant is realized.

The system, as indicated earlier, is composed of a solar field of parabolic trough collectors whose characteristics are shown in Table 1, two tanks, one of them is the principal tank the other is for regulation, 3 pumps, an auxiliary heating component that compensates the lack of heat of the fluid supplied by the tank when it is necessary and finally a heat exchanger. The configuration of the simulated solar plant is shown in Figure Fig. 1.

The dimensioning of the station is done on the basis of the temperature required at the outlet of the heat exchanger subsystem.

The thermal energy given to the load (to the heat exchanger) can be calculated by:

$$\dot{Q}_{load} = \dot{m}_{fl} C_{pfl} \Delta T_{load} \tag{44}$$

where C_{pfl} is the Therminol 62 specific heat capacity at required temperature and ΔT_{load} is the difference between the heat transfer fluid temperature at the input, $T_{in,exch}$, and the output, $T_{out,exch}$, of the heat exchanger. The required temperature of hot air at the outlet of the heat exchanger is 150 °C, therefore we set the input

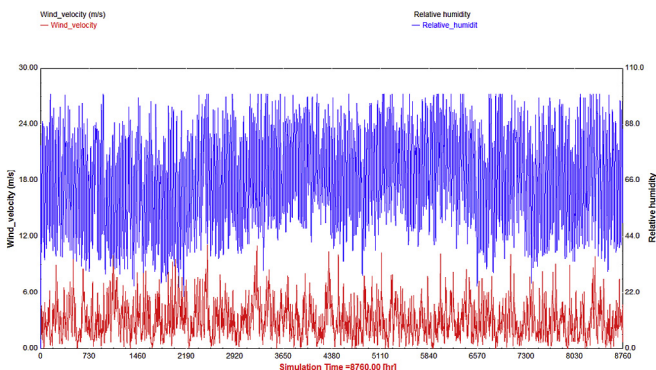


Fig. 6. Relative humidity and wind speed variation throughout the year.

Table 1
The parabolic trough features.

Feature	Value
Aperture area	28.8 m ²
Aperture width	1.2 m
Length	24 m
Focal length	0.65 m
Absorber tube diameter	28 mm
Cover diameter	45 mm
Concentration ratio	13.64
Rim angle	50°
Reflectivity, ρ	0.88
Emissivity, ε	0.15
Absorptivity, α	0.95
Transmittance, τ	0.89
Intercept factor, γ	0.85

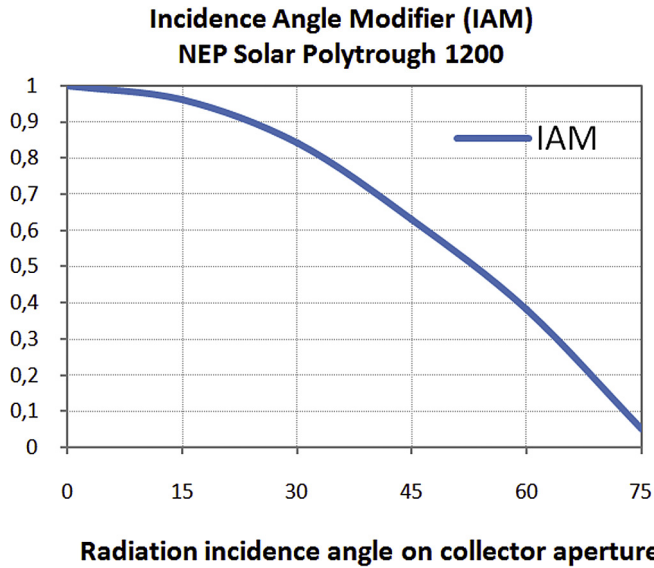


Fig. 8. Incidence angle modifier for NEP solar Polytrough1200 [41].

HTF temperature to $T_{in,exch} = 160$ °C. By setting the HTF flow rate to $\dot{m}_{fl} = 54$ kg/s at the pump P1 and considering $\Delta T_{load} = 90$ °C, the thermal energy $\dot{Q}_{load} = 10546,2$ kJ/s.

The volume of the storage tank is dimensioned using the equation:

$$V = \frac{Q_{str}}{\rho C_{pfl} \Delta T_{tank}} \quad (45)$$

where ρ and C_{pfl} are, respectively, the density and the specific heat capacity of the HTF, and Q_{str} is the desired energy to store in a determined time, it is expressed by:

$$Q_{str} = \dot{Q}_{load} \cdot t_{str} \quad (46)$$

With $t_{storage}$ is the time storage which consists of the average day time estimated to 8 h (28 800 s) and the desired charging night time that we set to 4 h (14 400 s). Therefore the estimated volume by considering 4 storage hours by night is approximately 3300 m³.

The HTF flow rate feeding the load from the tank, set by the pump P2, can be regulated according to the night time storage desired, and can be expressed by:

$$\dot{m}_{fl,tank} = \frac{Q_{str}}{C_{pfl} \Delta T_{tank} t_{str}} \quad (47)$$

By considering the charging time of 6 h (21 600 s) by night, the required flow is approximately $\dot{m}_{fl,tank} = 53,26$ kg/s for the volume tank of 3300 m³. Therefore, as a possible configuration, the solar collector field should contain 284 “Poly Trough 1200” parabolic trough collector in parallel and 5 in series in order to satisfy the requirements.

The heat exchanger is dimensioned using equations demonstrating the heat transfer in a counter-flow configuration.

Therefore using equation (31), and by calculating the difference between the output enthalpy and the input enthalpy for the HTF in the hot side of the heat exchanger, knowing that the flow rate of the HTF is set by the pump P2 to $\dot{m}_{fl} = 53,26$ kg/s, we found that $\dot{Q}_{exch} = 8388.45$ kJ/s. In our case, the required temperature of the air is about 150 °C, the calculation at the heat exchanger leads to an inlet HTF temperature required of 160 °C, assuming that the air enters the heat exchanger at 70 °C, the value of $\Delta T_{exch,ml}$ expressed

Table 2
The main properties of the HTF.

Feature	Value
Thermal conductivity, k	0.11 W/m K (W/m °C)
Kinematic viscosity, ν	1.26 mm ² /s
Density, ρ	870 kg/m ³
Heat capacity, C_p	2.2 kJ/kg K (kJ/kg °C)
Thermal diffusivity, $\alpha = k/\rho C_p$	6.22×10^{-5} m ² /s

Average properties at operating range of 100–220 °C temperature.

in equation (32) is calculated, thus by using equation (33), we can find that the value of the overall heat transfer coefficient for the heat exchanger needed is about $(U_{exch} A_{exch}) = 420,68$ kJ/s K (kJ/s °C).

Then, the calculation of the difference between output and input enthalpies of the air at the heat exchanger can conduct to the value of the flow rate of the air \dot{m}_{air} flowing over the heat exchanger. The calculation shows that $\dot{m}_{air} = 95,3$ kg/s.

6. Results and discussion

The operation of the plant is simulated with TRNSYS packages, using the components of both the standard library and TESS library (Thermal Energy Systems Specialists). The simulations have been carried out using a time step of 1 h (3600 s). The system performance can be predicted for whatever time basis. Dynamic simulations allow analyzing the fluctuations in temperatures and energy flows resulting from the selected control strategies and from the variation of solar energy available.

Fig. 9 presents the plant performance during the first week of January. It shows the variation of temperatures and the DNI throughout the week, we can see that the temperature at the output of the collectors field (red curve) varies in concordance with the variation of the DNI radiation (turquoise curve) that correspond approximately to 8 h per day, the pink curve presents the variation of the HTF temperature at the tank outlet that feeds the load. The blue line shows the air temperature required at the outlet of the cold side of the heat exchanger, corresponding to 150 °C, from 8:30 to 00:00 h, while the orange line shows the HTF temperature that corresponds to 160 °C, required to be delivered to the heat exchanger at the plant time operation.

In the following discussions, dynamic results will be summarized showing the autumn equinox as representative day. The trends still similar by changing the selected day, but the temperatures and energy flow values may significantly vary.

Fig. 10 shows that the PTC outlet temperature varies as a

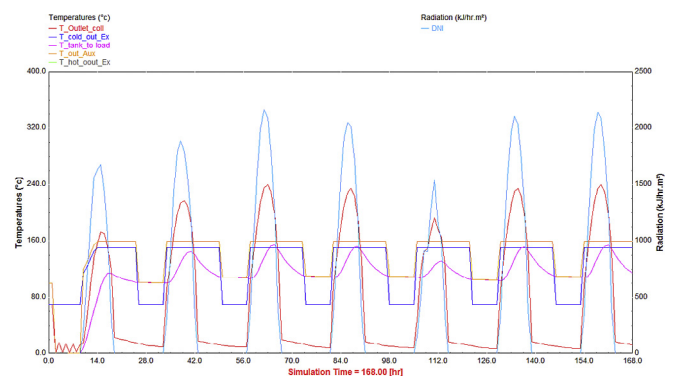


Fig. 9. The variation of different temperatures and of the DNI in the first week of January.

function of solar radiation availability. The maximum temperature reached by the solar collector field on this day is 290 °C, while the one at the top of the tank is 160 °C.

The maximum thermal power yielded by the solar field (blue curve) reaches 17,5 MW as shown in Fig. 11, it can be seen in this figure that when power begins to increase at the output of the solar field, and after a short time, power at the output of the storage tank (green curve) increases also and vice versa. Whereas at the auxiliary heater (red curve) the power varies in order to cover the mismatch between the requirement power in load and the supplied one by the storage tank, therefore the operation conditions of the plant are insured.

The HTF flow rate into the solar field is set by the pump P1, it is stabilized in a constant value during the time operation of the plant as illustrated in Fig. 12, thus during the central hours of the day a significant increase of PTCs efficiency is detected, reaching a maximum of 0.56.

Fig. 13 illustrates the variation of the exergy flows for the selected autumn day. A significant increase concerning the sun exergy flow (yellow curve) is detected during daytime, which reaches a maximum of 28 MW. This increase in the exergy coming from the sun determines a general growth of the exergy output at the solar field (blue spotted curve). The available exergy in the plant (green dashed curve), that reaches a maximum of 29.5 MW, consists of the exergy coming from the sun, the exergy given by the solar field and the one given by auxiliary heater, Hence this measure illustrates a significant increase during the daytime and a decrease to reach lowest values by night during the solar plant operation.

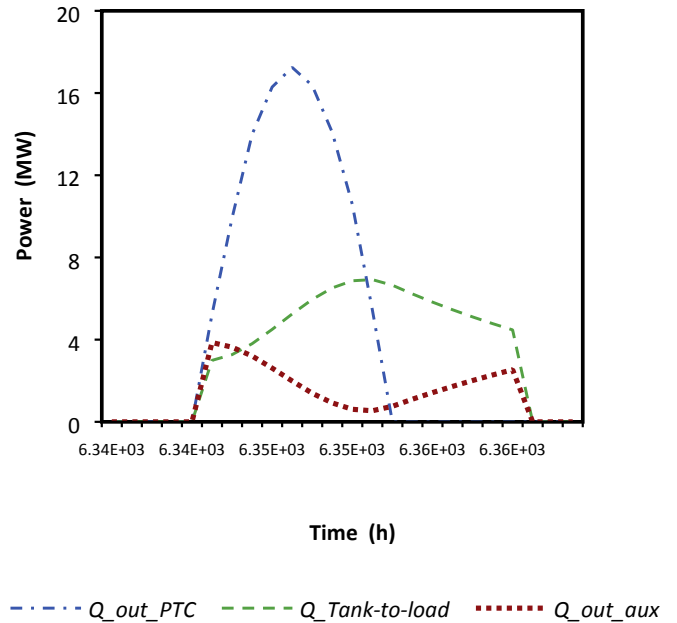


Fig. 11. Energy flows of the system in the autumn equinox.

The exergy efficiencies of the solar field with and without presence of the auxiliary heater in the plant are shown in Fig. 14. The exergetic efficiency increases significantly during daytime. The

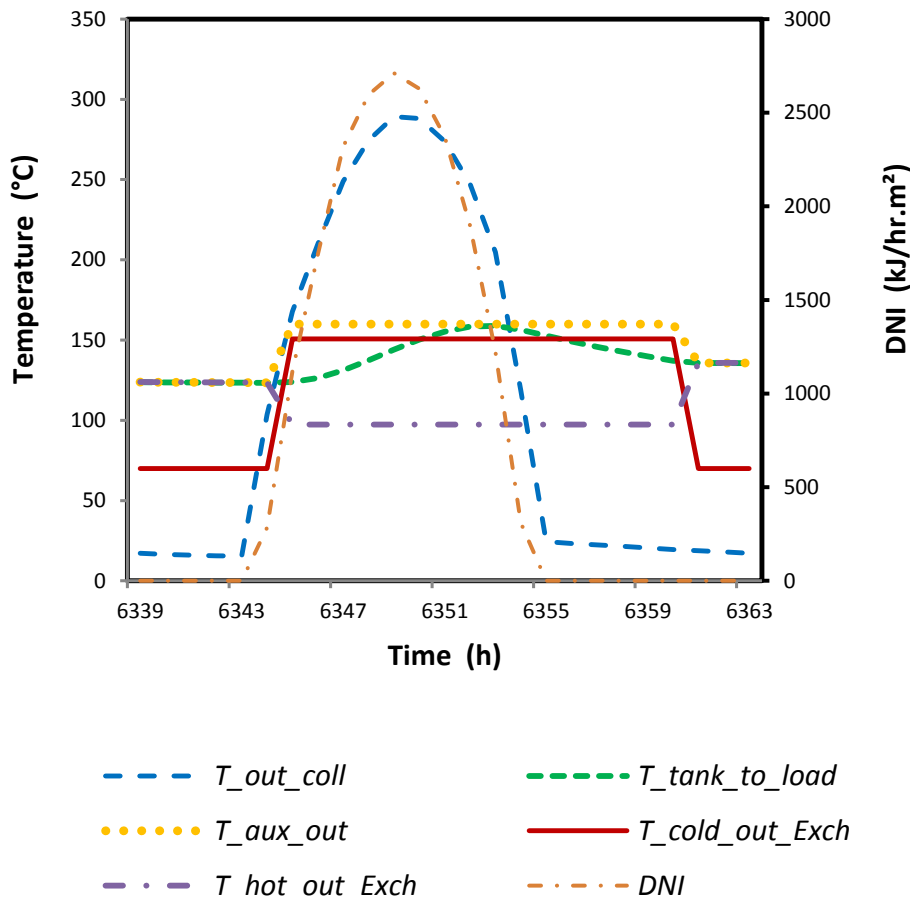


Fig. 10. The variation of different temperatures and of the DNI during the autumn equinox.

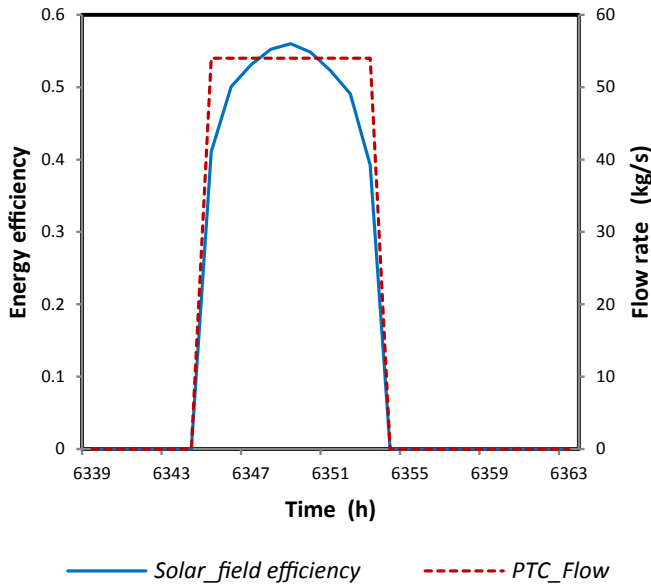


Fig. 12. Energy efficiency of the solar field and flow rate in the autumn equinox.

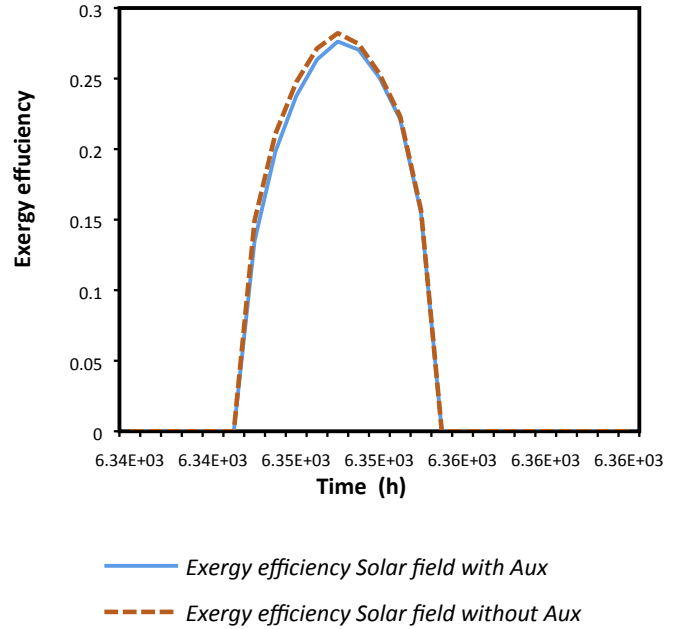


Fig. 14. Exergy efficiency of the solar field in the autumn equinox.

high exergetic efficiencies achieved in the solar collectors field are actually allowed by the high temperatures reached. In fact, the exergy efficiency increases when the temperature difference between the heat source (T_s) and the HTF (T_{out}) decreases, showing a maximum of 0.28 in the existence of the auxiliary heater and 0.285 in its absence. It is worth noting that for the calculation of exergy efficiency of the solar collectors field, the approach based on equations (8) and (9), the most common in literature is used.

For whatever component of the system, the exergy balance can be written. In Fig. 15 the irreversibility of the solar field subsystem which calculated by considering the exergy destruction is shown, a

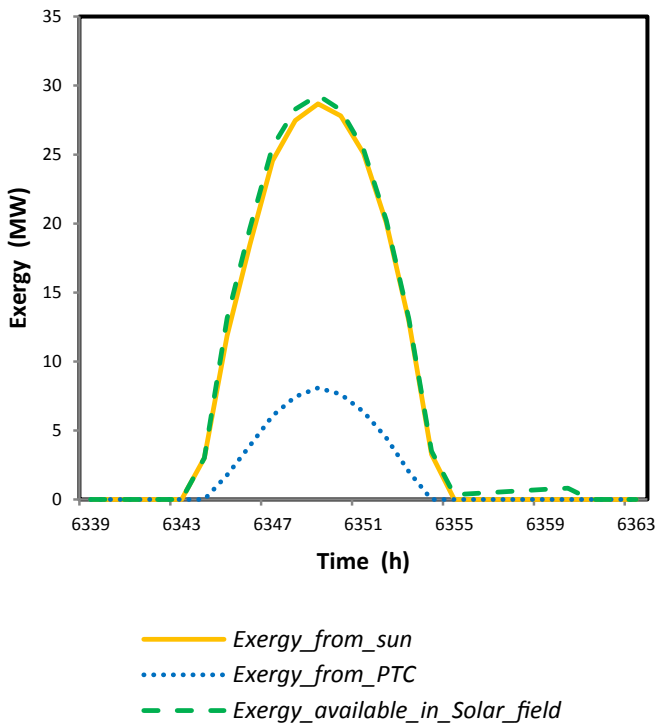


Fig. 13. Exergy flow in the autumn equinox.

peak of 21 MW is achieved with a significant increase during the sunlight. The entropy rate of the solar field is also illustrated, it clearly appears that its variation is in accordance with the variation of the irreversibility during the selected day with a maximum of 0.068 MW/K.

Results of the simulations are also illustrated on a monthly basis in order to perform energetic analyses of the system aiming at investigating performance parameters variations throughout the year. Fig. 16 shows the monthly energy flows at different components. The green lines show the monthly energy rate to load from the storage tank which increases during summer and achieves a maximum of 2.93 GWh on May, this energy becomes lower during winter as it varies in accordance with the variation of energy coming from the sun throughout the year. Conversely, the energy rate delivered to the HTF at the auxiliary heater, which is illustrated by the orange lines, is lower during summer and higher during winter. It is an expectable finding because of complementary roles of the storage tank and the auxiliary heater. Moreover, the blue lines show the amount of energy transferred at the heat exchanger.

The thermal efficiency plant is defined by equation (41), the exergy efficiency of the plant is presented as on equation (42) and the solar fraction is calculated using equation (43).

The monthly efficiencies and the solar fraction of the plant are presented in Fig. 17. The plant efficiency, dark blue line, is around 52%, the plant exergy efficiency is about 24% whereas the orange line presenting the solar fraction is around 56%.

It can be observed that in summer months efficiencies are low despite the high solar resources, it is due to the wasted energy excess. During the winter months, because of the lack of solar irradiation and also due to the relatively high demand, it can be seen that solar energy contribution is reduced. Noting that the higher the solar fraction the lower the efficiencies as illustrated in Fig. 17.

A significant part of this environmental impact assessment can be done using the CO₂ emissions due to combustion at the auxiliary heating component. Fig. 18 presents the monthly emissions of CO₂ and their equivalent for the operation of the storage tank of two fuels, natural gas and coal, at the auxiliary heating and the equivalent of these emissions for the operation of the storage tank. We

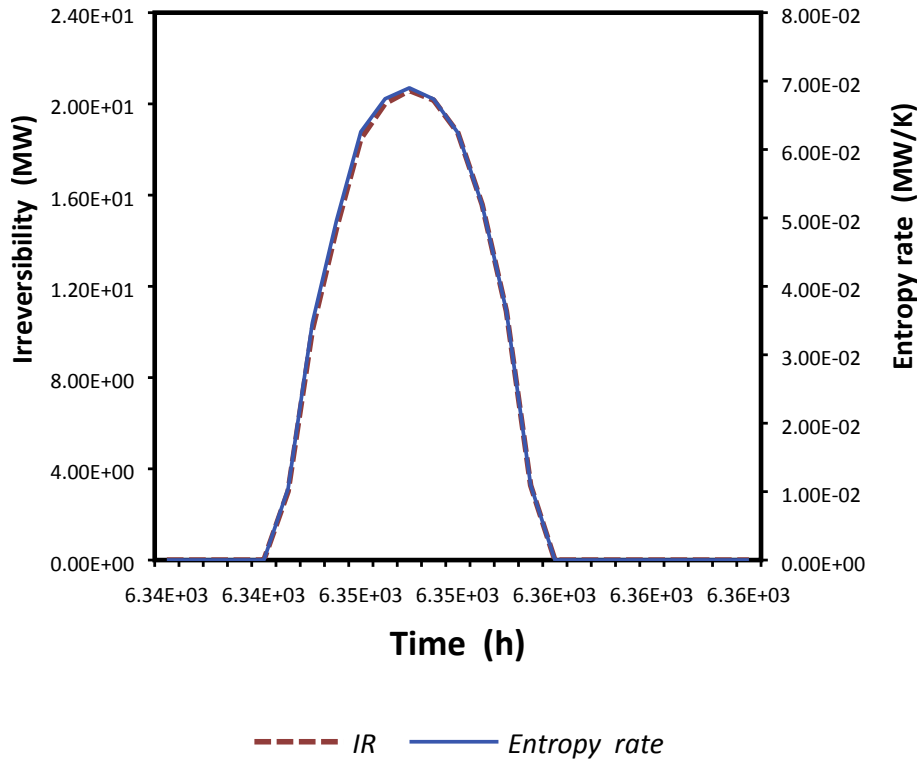


Fig. 15. Irreversibility and entropy rate in the autumn equinox.

can easily see that the emission quantity resulting from the coal combustion is much higher than the natural gas one. The coal combustion releases about 70% CO₂ emission more than natural gas. Taking the case where the plant uses natural gas, the cleanest of the two fuels, in August for example, Fig. 16 shows that the energy delivered to the fluid by the heating system is 1.69 GWh, Fig. 18 shows that the equivalent of this amount of energy is 345.98 tonnes

of CO₂ emitted into the atmosphere, while the amount of the energy supplied by the storage tank during this month is 1.63 GWh which makes us avoiding an equivalent of CO₂ of 333.14 tonnes. As a result, during the month of August, CO₂ emissions were reduced in that amount, comparing to the case where the only mean of air heating is the combustion of natural gas.

Annually an amount of 3.53 kt (kilotons = 1000 tonnes) of CO₂ is

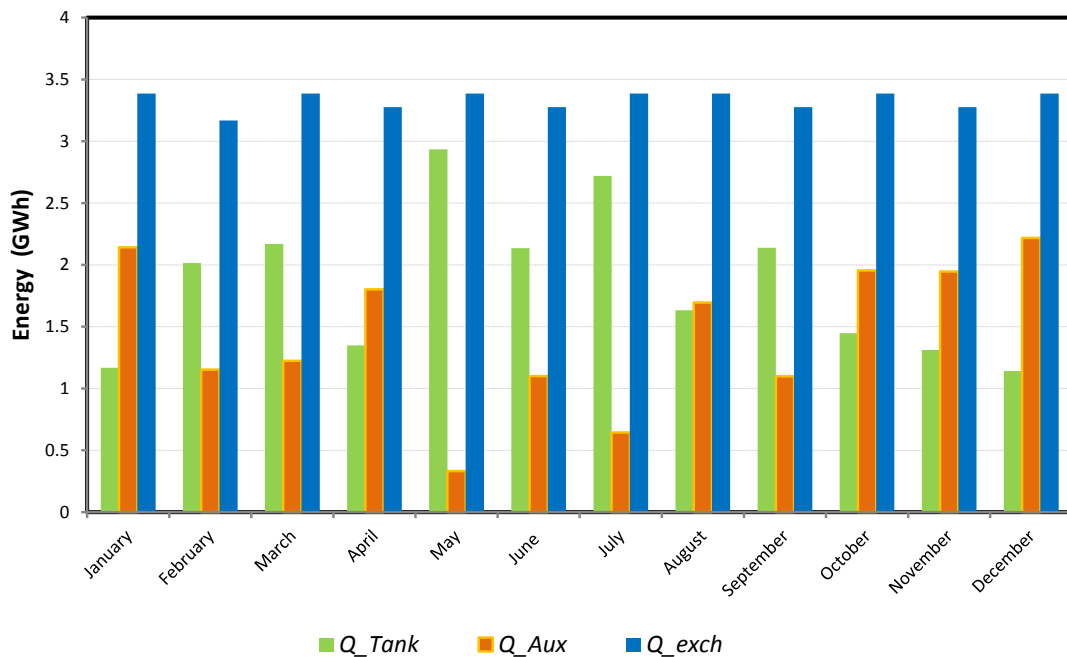


Fig. 16. The monthly energy at different components.

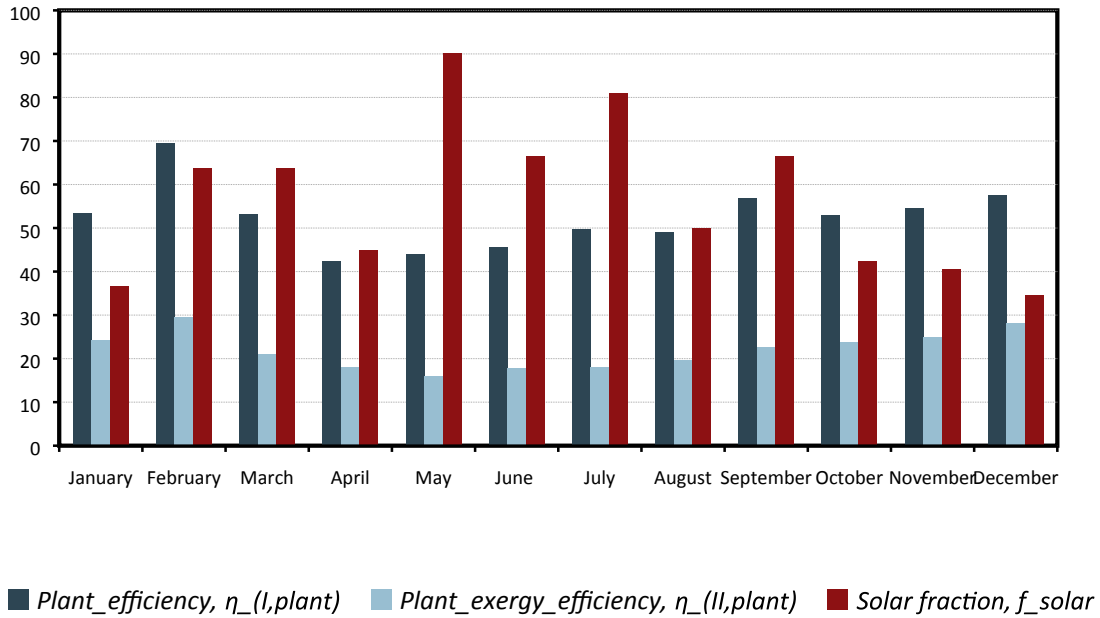


Fig. 17. The monthly efficiencies and the solar fraction of the plant.

released at the auxiliary heater when the natural gas is adopted as fuel, while the use of coal leads to release an amount of 5.97 kt.

Fig. 19 presents the monthly cost comparison between the two fuels; the coal and the natural gas. It clearly illustrates that the monthly cost of the natural gas is much higher than the one of the coal. The cost of each fuel evolves throughout months in concordance with the evolution of the energy needed at the auxiliary heater. Thus The factory will spend annually an amount of \$249955 by burning natural gas while this amount can be reduced about three times to become \$83780 by using coal. Therefore, we can expect that interest in using coal tends to increase because of the

higher natural gas price. Some factories, for more reducing the cost of heating, use a mixture of coal and Refuse-derived fuel (RDF) [44] releasing enormous quantities of toxic gases and ash causing serious adverse environmental and health impacts, especially in developing countries where there is a lack of legislative regulation regarding the emissions ceiling amounts that each undertaking must not exceed. The incorporation of such a solar thermal plant makes it possible to reduce an amount of \$319975 when the fuel used is natural gas or \$107249 when coal is used at the auxiliary heater and makes that a great part of emissions can be avoided regardless the nature of the fuel chosen.

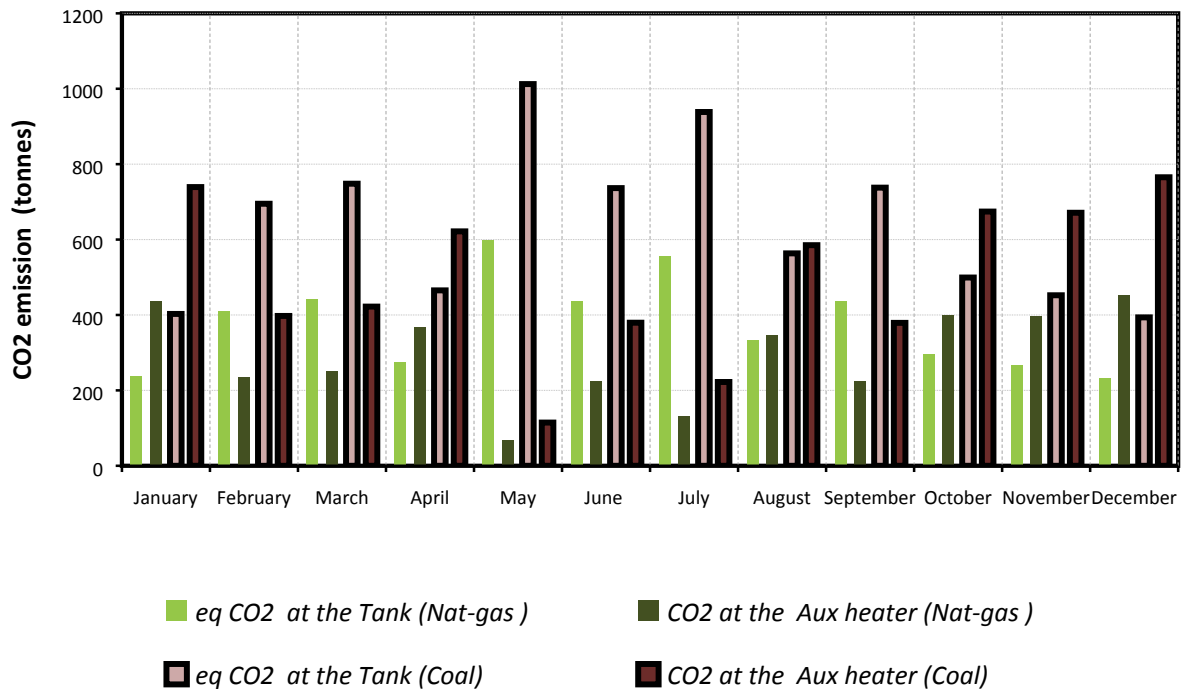


Fig. 18. CO₂ emissions due to natural gas and coal combustion at the auxiliary heating component and its equivalent for the storage tank.

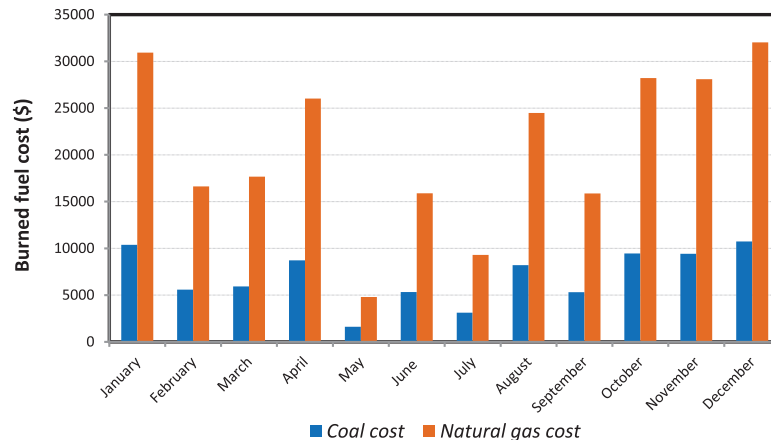


Fig. 19. The monthly cost of the chosen fuel to be burned at the auxiliary heater.

In Morocco by 2014, coal, which is mostly used for electricity generation, is among the main sources of CO₂ emission by (22.6%) [38] of total emissions, and natural gas by (4.8%) [38]. Contrary to expectations, according to the IEA report, the strongest increase in emissions came from natural gas, as a consequence of significant consumption growth (30 times over) compared with 2002 [38], despite its high price. While emissions from coal decreased by 12.4% [38].

7. Conclusions

A thermal station based on parabolic trough collectors (brand NEP Solar, model PolyTrough1200) has been considered for the purpose of producing hot air for an industrial process. Its performance has been simulated using TRNSYS software feeding the meteorological data of AitBaha-Agadir site, in Morocco.

The analysis results show in detail the simulated thermal energy yield of all the main plant components and its control operation, as well. Simulations have been performed on daily, weekly and monthly bases.

Main findings of this study are the following:

- The set-point for the outlet air temperature at the heat exchanger is 150 °C. As the thermal energy supplied by the tank is not enough to keep it during the whole daily operating time, 8:30 h to 00:00 h, the auxiliary heater is necessary to supply the additional heat needs.
- The solar gain at the collector field during daytime allows achievement of higher temperatures than the set-point, determining an increase of energetic efficiency and of thermal energy recovered in the heat exchanger subsystem.
- The exergetic analysis at the solar field shows that solar radiation allows an exergy increase in the HTF circulating through the PTCs. This contribution increases significantly during daytime, and is still the main exergy contribution compared to the auxiliary heater exergy, which appears lower by night.
- The plant energy and exergy efficiencies decrease when the solar fraction of the plant increases.
- The monthly energy rate delivered to the HTF at the auxiliary heater is lower during the summer and higher during the winter ones, conversely of the storage tank outlet energy.
- The contribution from the heat storage tank is inversely related to the amount of CO₂ emissions resulting from both, natural gas or coal combustion at the auxiliary heater.

- Coal combustion in the auxiliary heater releases 70% higher CO₂ emissions than natural gas but the annual cost of coal combusted in the auxiliary heater is lower by about 66.5% regarding the natural gas cost.
- Those CO₂ emissions resulting at the auxiliary heater can be reduced by up to 57% annually through the use of a small sized parabolic trough plant.
- contrary to expectation natural gas consumption increases significantly while coal use decreases according to the IEA 2014 report.
- The integration of such small sized parabolic trough plants into industry can somehow decrease the dependence of Morocco on imported energy resources.

Acknowledgment

This work was financially supported by IRESEN (Institut de Recherche en Energie Solaire et Energies Nouvelles, Morocco) in the framework of the InnoTherm1 project: CSP Ait Baha. The authors express their acknowledgments to Dr. Eduardo Zarza head of the PSA-(Plataforma Solar de Almeria)-R&D Unit on Solar Concentrating Systems in Spain, for his useful comments to improve the paper.

References

- [1] I. Arto, I. Capellán-Pérez, R. Lago, G. Bueno, R. Bermejo, The energy requirements of a developed world, *Energy Sustain. Dev.* 33 (2016) 1–13, <http://dx.doi.org/10.1016/j.esd.2016.04.001>.
- [2] R. Silva, F.J. Cabrera, M. Pérez-García, Process heat generation with parabolic trough collectors for a vegetables preservation industry in Southern Spain, *Energy Procedia* 48 (2014) 1210–1216, <http://dx.doi.org/10.1016/j.egypro.2014.02.137>.
- [3] H. Schweiger, J.F. Mende, B. Nikolaus, K. Hennecke, G. Prieto, C. Merce, H. Gonsalves, The potential of solar heat industrial processes, *A state Art Rev. Spain Potugal, EuroSun* (2000), <http://dx.doi.org/10.1017/CBO9781107415324.004>.
- [4] S. Kalogirou, The potential of solar industrial process heat applications, *Appl. Energy* 76 (2003) 337–361, [http://dx.doi.org/10.1016/S0306-2619\(02\)00176-9](http://dx.doi.org/10.1016/S0306-2619(02)00176-9).
- [5] A. Fernandez-Garcia, E. Zarza, L. Valenzuela, M. Pérez, Parabolic-trough solar collectors and their applications, *Renew. Sustain. Energy Rev.* 14 (2010) 1695–1721, <http://dx.doi.org/10.1016/j.rser.2010.03.012>.
- [6] AEA (American Energy Assets), Industrial Process Steam Generation Using Parabolic Trough Solar Collection, Public Interest Energy Research (PIER) Program, 2010. <http://www.energy.ca.gov/2011publications/CEC-500->.
- [7] H. Price, E. Lüpfert, D. Kearney, E. Zarza, G. Cohen, R. Gee, R. Mahoney, Advances in parabolic trough solar power technology, *J. Sol. Energy Eng.* 124 (2002) 109, <http://dx.doi.org/10.1115/1.1467922>.
- [8] IEA-ETSAP, and IRENA, <http://www.etsap.org/web/Supply.asp> and www.irena.org/Publications.
- [9] NREL, <http://www.nrel.gov/csp/solarpaces/>.

- [10] M.W. Edenburg, Performance analysis of a cylindrical parabolic focusing collector and comparison with experimental results, *Sol. Energy* 18 (1976) 437–444, [http://dx.doi.org/10.1016/0038-092X\(76\)90010-4](http://dx.doi.org/10.1016/0038-092X(76)90010-4).
- [11] M.E. Rojas, M.C. De Andre, L. Gonza, Designing capillary systems to enhance heat transfer in LS3 parabolic trough collectors for direct steam generation (DSG) 82 (2008) 53–60, <http://dx.doi.org/10.1016/j.solener.2007.04.005>.
- [12] N. Naeeni, M.A. Yaghoubi, Analysis of wind flow around a parabolic collector (1) fluid flow 32 (2007) 1898–1916, <http://dx.doi.org/10.1016/j.renene.2006.10.004>.
- [13] G.C. Bakos, Design and construction of a two-axis Sun tracking system for parabolic trough collector (PTC) efficiency improvement 31 (2006) 2411–2421, <http://dx.doi.org/10.1016/j.renene.2005.11.008>.
- [14] S.M. Jeter, Analytical determination of the optical performance of practical parabolic trough collectors from design data, *Sol. Energy* 39 (1987) 11–21.
- [15] C. You, W. Zhang, Z. Yin, Modeling of fluid flow and heat transfer in a trough solar collector, *Appl. Therm. Eng.* 54 (2013) 247–254, <http://dx.doi.org/10.1016/j.applthermaleng.2013.01.046>.
- [16] S. Quoilin, M. Orosz, H. Hemond, V. Lemort, Performance and design optimization of a low-cost solar organic Rankine cycle for remote power generation, *Sol. Energy* 85 (2011) 955–966, <http://dx.doi.org/10.1016/j.solener.2011.02.010>.
- [17] F.A. Al-sulaiman, F. Hamdullahpur, I. Dincer, Performance assessment of a novel system using parabolic trough solar collectors for combined cooling, heating, and power production, *Renew. Energy* 48 (2012) 161–172, <http://dx.doi.org/10.1016/j.renene.2012.04.034>.
- [18] Y.-L. He, D.-H. Mei, W.-Q. Tao, W.-W. Yang, H.-L. Liu, Simulation of the parabolic trough solar energy generation system with organic rankine cycle, *Appl. Energy* 97 (2012) 630–641, <http://dx.doi.org/10.1016/j.apenergy.2012.02.047>.
- [19] TRNSYS, Libraries of User Components for TRNSYS 17.
- [20] M. Borunda, O.A. Jaramillo, R. Dorantes, A. Reyes, Organic rankine cycle coupling with a parabolic trough solar power plant for cogeneration and industrial processes, *Renew. Energy* (2016), <http://dx.doi.org/10.1016/j.renene.2015.08.041>.
- [21] S.A. Kalogirou, Parabolic trough collectors for industrial process heat in 27 (2002) 813–830.
- [22] R. Silva, M. Pérez, A. Fernández-garcía, Modeling and co-simulation of a parabolic trough solar plant for industrial process heat, *Appl. Energy* 106 (2013) 287–300, <http://dx.doi.org/10.1016/j.apenergy.2013.01.069>.
- [23] A. John, w. A. Beckman, *Solar Engineering of Thermal Processes*, J. Wiley and Sons, 1991.
- [24] N. Singh, S.C. Kaushik, R.D. Misra, Exergetic analysis of a solar thermal power system, *Renew. Energy* 19 (2000) 135–143, [http://dx.doi.org/10.1016/S0960-1481\(99\)00027-0](http://dx.doi.org/10.1016/S0960-1481(99)00027-0).
- [25] S.K. Tyagi, S. Wang, M.K. Singhal, S.C. Kaushik, S.R. Park, Exergy analysis and parametric study of concentrating type solar collectors, *Int. J. Therm. Sci.* 46 (2007) 1304–1310, <http://dx.doi.org/10.1016/j.ijthermalsci.2006.11.010>.
- [26] C. Xu, Z. Wang, X. Li, F. Sun, Energy and exergy analysis of solar power tower plants, *Appl. Therm. Eng.* 31 (2011) 3904–3913, <http://dx.doi.org/10.1016/j.applthermaleng.2011.07.038>.
- [27] Ö. Kaşka, Energy and exergy analysis of an organic Rankine for power generation from waste heat recovery in steel industry, *Energy Convers. Manag.* 77 (2014) 108–117, <http://dx.doi.org/10.1016/j.enconman.2013.09.026>.
- [28] F. Calise, D. Capuano, L. Vanoli, Dynamic Simulation and Exergo-economic Optimization of a Hybrid Solar–geothermal Cogeneration Plant, 2015, pp. 2606–2646, <http://dx.doi.org/10.3390/en8042606>.
- [29] F. Calise, A. Palombo, L. Vanoli, A finite-volume model of a parabolic trough photovoltaic/thermal collector: energetic and exergetic analyses, *Energy* 46 (2012) 283–294, <http://dx.doi.org/10.1016/j.energy.2012.08.021>.
- [30] M. Liu, N.H. Steven Tay, S. Bell, M. Belusko, R. Jacob, G. Will, W. Saman, F. Bruno, Review on concentrating solar power plants and new developments in high temperature thermal energy storage technologies, *Renew. Sustain. Energy Rev.* 53 (2016) 1411–1432, <http://dx.doi.org/10.1016/j.rser.2015.09.026>.
- [31] M. Medrano, A. Gil, I. Martorell, X. Potau, L.F. Cabeza, State of the art on high-temperature thermal energy storage for power generation. Part 2-Case studies, *Renew. Sustain. Energy Rev.* 14 (2010) 56–72, <http://dx.doi.org/10.1016/j.rser.2009.07.036>.
- [32] A. Gil, M. Medrano, I. Martorell, A. Lázaro, P. Dolado, B. Zalba, L.F. Cabeza, State of the art on high temperature thermal energy storage for power generation. Part 1-Concepts, materials and modellization, *Renew. Sustain. Energy Rev.* 14 (2010) 31–55, <http://dx.doi.org/10.1016/j.rser.2009.07.035>.
- [33] Y. Lechón, C. De Rúa, R. Sáez, Life cycle environmental impacts of electricity production by solarthermal power plants in Spain 130 (2008) 1–7, <http://dx.doi.org/10.1115/1.2888754>.
- [34] Y. Hu, G. Xu, C. Xu, Y. Yang, Thermodynamic analysis and techno-economic evaluation of an integrated natural gas combined cycle (NGCC) power plant with post-combustion CO₂ capture, *Appl. Therm. Eng.* 111 (2017) 308–316, <http://dx.doi.org/10.1016/j.applthermaleng.2016.09.094>.
- [35] M.V.J. Suresh, K.S. Reddy, A.K. Kolar, 4-E (Energy, Exergy, Environment, and Economic) analysis of solar thermal aided coal-fired power plants, *Energy Sustain. Dev.* 14 (2010) 267–279, <http://dx.doi.org/10.1016/j.esd.2010.09.002>.
- [36] A. Li, M. Hu, C. Sun, Z. Li, Optimal CO₂ abatement pathway with induced technological progress for Chinese coal-fired power industry, *Energy Sustain. Dev.* (2014), <http://dx.doi.org/10.1016/j.esd.2016.03.009>.
- [37] W.J. Kostowski, S. Uson, Thermo-economic assessment of a natural gas expansion system integrated with a co-generation unit, *Appl. Energy* 101 (2013) 58–66, <http://dx.doi.org/10.1016/j.apenergy.2012.04.002>.
- [38] International Energy Agency, Morocco 2014, (2014) 13.
- [39] ONHYM (Office National des Hydrocarbures et des Mines) National Office of Hydrocarbons and Mines in Morocco, www.onhym.com, (2012).
- [40] EIA, <http://www.eia.gov/>.
- [41] A. Giostri, M. Binotti, M. Astolfi, P. Silva, E. Macchi, G. Manzolini, Comparison of different solar plants based on parabolic trough technology, *Sol. Energy* 86 (2012) 1208–1221, <http://dx.doi.org/10.1016/j.solener.2012.01.014>.
- [42] Nep-Solar, <http://www.nep-solar.com/products/polytrough-1200>. <http://www.nep-solar.com/products/polytrough-1200>.
- [43] Therminol, <https://www.therminol.com/products>.
- [44] T. Kupka, M. Mancini, M. Irmer, R. Weber, Investigation of ash deposit formation during co-firing of coal with sewage sludge, saw-dust and refuse derived fuel, *Fuel* 87 (2008) 2824–2837, <http://dx.doi.org/10.1016/j.fuel.2008.01.024>.